

# Propagation of Ripples in Monte Carlo Models of Sputter Induced Surface Morphology

Emmanuel O. Yewande, Alexander K. Hartmann, and Reiner Kree

Institut für Theoretische Physik, Universität Göttingen,  
Friedrich-Hund Platz 1, 37077 Göttingen, Germany

(Dated: March 9, 2022)

Periodic ripples generated from the oblique incidence ion beam bombardment of solid surfaces have been observed to propagate with a dispersion in the velocity. We investigate this ripple behaviour by means of a Monte Carlo model of the erosion process, in conjunction with one of two different surface diffusion mechanisms, representative of two different classes of materials; one is a Arrhenius-type Monte Carlo method including a term (possibly zero) that accounts for the Schwoebel effect, the other a thermodynamic mechanism without the Schwoebel effect. We find that the behavior of the ripple velocity and wavelength depends on the sputtering timescale, qualitatively consistent with experiments. Furthermore, we observe a strong temperature dependence of the ripple velocity, calling for experiments at different temperatures. Also, we observe that the ripple velocity vanishes ahead of the periodic ripple pattern.

PACS numbers: 05.10.-a, 68.35.-p, 79.20.-m

## I. INTRODUCTION

There has been much scientific activity for quite some time now, on the features of surface morphology resulting from the bombardment of a solid surface by a collimated beam of intermediate energy ions, at normal and oblique incidence to the solid surface [1, 2]. The phenomenon is an essential constituent of several surface analysis, processing and fabrication techniques, such as ion beam aided deposition, surface catalysis, sputter cleaning, etching and deposition.

Normal incidence ion bombardment of non-metallic substrates often results in an interlocking grid of hillocks and depressions, which have been demonstrated to be an attractive alternative to the spontaneous growth of self-organized quantum dots on semiconductor surfaces in the Stranski-Krastanov growth mode [3]. Oblique incidence ion bombardment of such non-metallic substrates, however, gives rise to the formation of quasiperiodic ripples [4, 5, 6, 7, 8, 9, 10, 11] with orientation that depends on the angle of incidence of the ion beam. For incidence angles less than a critical angle,  $\theta_c$  [12], the wavevector of the ripples is parallel to the projection of the ion beam direction on the surface plane while for incidence angles greater than  $\theta_c$ , the wavevector of these ripples is oriented perpendicular to the projection of the ion beam direction on the surface plane. On the other hand, ripples are observed on metallic substrates at normal incidence ion bombardment, and these ripples are rotated by changing the substrate temperature [13, 14, 15]; a probable consequence of the symmetry-breaking anisotropy in surface diffusion. The wavelengths of the observed ripples, in all cases, is of the order of tenths of micrometers.

However, a number of experimental studies [16, 17, 18,

19] have demonstrated that under certain ion bombardment conditions, ripples are not formed; the surface undergoes kinetic roughening with interesting scaling properties. All these observations point to the possibility of several phases in the surface topography evolution, with phase boundaries defined by the bombardment conditions, and with little or no dependence on the material composition, surface chemistry, defects or chemical reactions on the surface. These features are understood, from insightful theoretical descriptions [2, 20, 21], as being governed by the interplay and competition between the dynamics of surface roughening on the one hand and material transport during surface migration on the other. Ion bombardment tends to roughen the surface, while surface diffusion leads, in general, to surface relaxation [4, 5]. For sufficiently low ion energies, the sputtering phenomenon is the dominating mechanism [2]. However, if the flux is low at such energies, then the enhanced defect mobility can result to domination by surface diffusion which may cause the overall scaling behavior of the surface profile to be uniquely determined by the nonequilibrium biased diffusion current, independently of the microscopic origin [22].

Recently surface ripples generated during Gallium ion beam erosion of Silicon were observed to propagate with a ripple velocity that scales with the ripple wavelength as  $v \propto \lambda^k$ , where  $k \neq 0$  initially, and  $k = -1.5$  after a crossover wavelength  $\lambda_c \approx 100\text{nm}$  [23]. This velocity dispersion has been ascribed to an indication of a continuous transition to a rising non-linear contribution in surface erosion [2, 23]. Motivated by this experimental result, we study ripple propagation by means of a recently introduced, discrete  $(2+1)$  dimensional Monte Carlo (MC) model [24] of the sputtering process, and two different solid on solid models of surface diffusion; for details see below. We focus on intermediate times, where the transition from linear to non-linear regimes occur. Our results corroborate the experimental observation, but in addi-

---

Electronic address: yewande@theorie.physik.uni-goettingen.de

tion, we find that, at high temperatures, the ripples first come to rest before they are completely wiped out by the increasing non-linear contributions.

The rest of the paper is organized as follows. First, we state our simulation model, i.e. how the sputtering process and the different diffusion mechanisms are implemented. Then we explain, how we study the evolution of the ripples. In the main section, we show our simulation results. We finish with our conclusions and an outlook.

## II. EROSION AND SURFACE MIGRATION

According to Sigmund's sputtering theory [25], the rate at which material is removed from a solid surface, through the impact of energetic particles, is proportional to the power deposited there by the random slowing down of particles. The average energy  $E(r^0)$  deposited at surface point  $r^0 = (x^0, y^0, z^0)$  is given by the Gaussian distribution

$$E(r^0) = \frac{1}{(2\pi)^{3/2}} \exp \left[ -\frac{(z^0 + d)^2}{2\sigma_z^2} - \frac{x^0^2 + y^0^2}{2\sigma_{xy}^2} \right] \quad (1)$$

where we have used the local Cartesian coordinate system of the ion with origin at the point of penetration and with the  $z$  axis coinciding with the ion beam direction;  $(z^0 + d)$  is the distance of the surface point, from the stopping point of ion, measured along the ion trajectory,  $\sqrt{x^0^2 + y^0^2}$  is the distance perpendicular to it;  $\sigma_z$  and  $\sigma_{xy}$  are the widths of the distribution parallel and perpendicular to the ion trajectory respectively;  $E$  is the total energy deposited,  $d$  is the average depth of energy deposition. Sigmund's formula is the basis for all theoretical treatments and analysis of experimental results so far.

### A. The Sputtering Process

Following [24], we simulate the sputtering process on a surface of size  $L^2$  with periodic boundary conditions, by starting an ion at a random position in a plane parallel to the plane of the initially flat surface, and projecting it along a straight trajectory inclined at angle  $\theta$  to the normal to the average surface configuration; at an azimuthal angle  $\phi$ . The ion penetrates the solid through a depth  $d$  and releases its energy, such that an atom at a position  $r = (x, y, h)$  is eroded (see Fig. 1 of [24]) with probability proportional to  $E(r)$ . It should be noted that, consistent with the assumptions of the theoretical models [2, 20, 21], this sputtering model assumes no evaporation, no redeposition of eroded material, no preferential sputtering of surface material at point of penetration, and surface is defined by a single valued, discrete time dependent height function  $h(x, y, t)$  (solid-on-solid model, SOS). The time  $t$  is measured in terms of the ion fluence; i.e. number of incident ions per two-dimensional lattice site  $(x, y)$ . We used incidence angle  $\theta = 50^\circ$ , azimuthal angle  $\phi = 22.0^\circ$ ,

$d = 6.0$ ,  $\sigma_z = 3.0$ ,  $\sigma_{xy} = 1.5$ , as obtained by SRIM [26] for 5keV  $Xe^+$  ions on graphite and rescaling all lengths by a factor 2. This should give according to the linear theory of Bradley and Harper a value  $\sigma_c = 68$  [12]. We have chosen  $\sigma$  to be  $(2\pi)^{3/2} \sigma_c^2$ , which leads to high sputtering yields  $Y \approx 7.0$  compared to experiments like [11], where  $Y = 0.3; \dots; 0.5$ , i.e. increasing the efficiency of the simulation. According to the Bradley Harper theory, the ripple wavelength scales like  $\lambda \propto Y^{1/2}$  so that we expect patterns with correspondingly smaller length scales in our simulations. This we have to remember when quantitatively interpreting the result. Anyway, the general phenomena observed in the simulation are not affected by this choice.

Our model of the sputtering mechanism sets the time scale of the simulation, and allows comparison with experiments. Additionally, also moves of atoms mimicking surface diffusion are performed, described now.

### B. The Hamiltonian and Arrhenius Models of Surface Diffusion

Surface migration is modelled as a thermally activated nearest neighbor hopping process, as in [27, 28]. A Monte Carlo acceptance/rejection procedure is used for this purpose. One diffusion step refers to a complete sweep of the lattice. Two different solid-on-solid models of surface diffusion in molecular beam epitaxy are used; the second one of them sensitive to the repulsion of a diffusing particle from a down step, and preferential diffusion in the uphill direction: the so-called Schwoebele effect.

The first model [27] is based on a thermodynamic interpretation of the diffusion process. For each step, a site  $i$  and one neighbour site  $j$  are randomly selected. The trial move is an atom hopping from  $i$  to  $j$ , i.e.  $h_i = h_i - 1$  and  $h_j = h_j + 1$ . We calculate the surface energy before and after the hop, through the energy of an unrestricted SOS model

$$E = \frac{J}{2} \sum_{\langle i, j \rangle} h_i h_j \quad (2)$$

$J$  is a coupling constant through which the nearest neighbor sites interact.  $h_i$  is the height variable at site  $i$ , and the summation is over the nearest neighbors on the 2-dimensional substrate.

The hop is allowed with the probability

$$p_{i \rightarrow j} = \min \left( 1, \exp \left[ -\frac{4 E_{i \rightarrow j}}{k_B T} \right] \right) \quad (3)$$

where  $4 E_{i \rightarrow j}$  is the energy difference between the initial and final states of the move.  $T$  is the substrate temperature, and  $k_B$  is the Boltzmann's constant. Although no exact mapping is possible we can estimate that a temperature  $k_B T = J \approx 0.2$  in this model corresponds roughly to the temperature used in the second model below. The estimate is based on a comparison of the pure

diffusion mechanism without sputtering such that they lead to comparable values of the roughness. Note that this temperature is below the roughening transition of this model [27]. This model does not prevent atoms from moving down over steps edges, hence no Schwoebel effect is present.

The second model is also based on a MC procedure and uses a formula known from kinetic MC mechanisms. For each step, again a site  $i$  and a nearest neighbor site  $j$  are chosen at random but now a hopping move is performed with a probability proportional to the hopping rate of an Arrhenius form

$$k(E; T) = k_0 \exp \left( -\frac{E}{k_B T} \right) \quad (4)$$

$E = E_{SB} + nnE_{NN} + E_S$  is an energy barrier to hopping, consisting of a Schwoebel barrier term  $E_{SB}$ , a substrate term  $E_S = 0.75\text{eV}$  and a nearest neighbor bonding of magnitude  $nnE_{NN} = nn0.18\text{eV}$ ; where  $nn$  is the number of in-plane nearest neighbors of the diffusing atom.  $E_{SB}$  is equal to some constant ( $0.15\text{eV}$  in this case. Note that we perform also runs for  $E_{SB} = 0$ , to compare with the thermodynamic model, see below), if the numbers of next-nearest neighbors in the plane beneath the hopping atom before ( $nnn_b$ ) and after ( $nnn_a$ ) the hop, obey  $4 = nnn_b > nnn_a$ ; and zero otherwise. Our temperature is measured in units of  $\text{eV} k_B^{-1}$  in this model, where  $T = 0.02\text{eV} k_B^{-1}$  corresponds to room temperature.  $k_0 = 2k_B T = \hbar$  is the vibrational frequency of a surface adatom, i.e. a hopping attempt rate,  $\hbar$  being Planck's constant. The hopping attempt rate is very high, with a corresponding low hopping probability resulting from Eq. 4, slowing down the simulation. Thus we incorporate the factor  $\exp(-E_S/k_B T)$  into the rescaled attempt rate such that the hopping rate reads

$$k(E; T) = k_1 \exp \left( -\frac{4E}{k_B T} \right) \quad (5)$$

where  $k_1 = k_0 \exp(-E_S/k_B T)$  is a much lower hopping attempt rate,  $4E = nnE_{NN} + E_{SB}$ . This physical attempt rate, in comparison with the ion current density used in experiments, determines the ratio between the number of sputtering steps and the number of surface diffusion steps made in the simulation. In the next section, we state the values we used for our simulations. A discussion of parameter optimization and a rescaling of the temperature with the parameters is given in [29] Note finally that for atoms on top of planes, which are far from down edges,  $E = 0$ , i.e. each hop is accepted, independently of the temperature.

### III. RIPPLE KINEMATICS

In experiments, we typically have  $N = 1 \times 10^{15} \text{atom s/cm}^2$  on the surface. Since the typical experimental ion current density is of the order

$F = 7.5 \times 10^{14} \text{ions/cm}^2 \text{s}$  [23], this implies a flux of  $\Phi = F/N = 0.75 \text{ion/atom s}$ . From the values given above, we get hopping attempt rates  $k_1$  of around 200 1/s for room temperature, hence 200 sweeps of the diffusion mechanism correspond to 0.75 ions per surface atom. Thus, we initiate a diffusion step every  $L^2 = k_1 = 0.0037 L^2$  erosion steps;  $L$  is the system size.

Initially, for times less than about 1.4 ions/lattice site, the surface is rough [24] and then the formation of ripples starts. In this paper we focus on the motion and time development of these ripples. In Fig. 1 the time development of a sample surface topology is shown for the first diffusion model. Initially ripples are formed. They propagate slowly and, due to the increasing influence of non-linear effects (note the scales at the right), disappear at longer times. The long-time behavior, where the ripples have disappeared, has already been studied in Ref. 24.

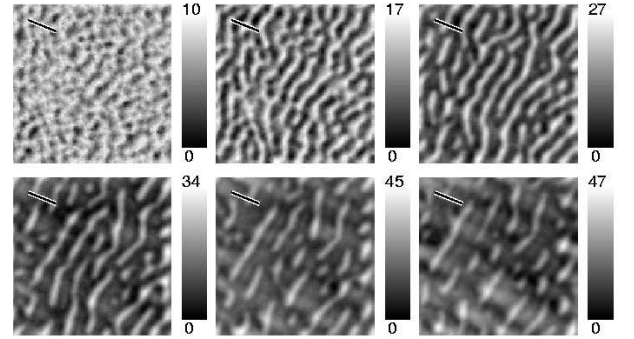


FIG. 1: Surface profiles at a substrate temperature of  $0.2 \text{J} k_B^{-1}$  and at different times. Starting from top-bottom, left-right,  $t = 0.5, 1.5, 4.0, 9.0, 14.0$  and  $20.0$  ions/atom. Ion beam direction, indicated by the bar, is perpendicular to ripple orientation. The scales show the surface height measured from the lowest height.

In order to monitor the ripple propagation on the computer, we assign the crest points of the ripples to clusters, and then monitor the motion of these clusters. A cluster of crest points is defined as the set of surface points with height  $h(x; y; t) > h_c$  and nearest neighbor distance  $l > l_c$ , where  $h_c$  and  $l_c$  are cut-off surface height and distance between neighboring cluster points respectively. We have chosen our cut-off height to be a function of the average height of the configuration  $\bar{h}$ , and the height difference  $h_d$  between the maximum and minimum of the surface; i.e.  $h_c = \bar{h} + p h_d$ , where  $p$  is some fixed percentage. In this way clusters with about the same proportionate sizes can be followed from the beginning of ripple formation until complete disappearance of the ripples. Furthermore, we have used  $l_c = 2$ . Different, unconnected ripples should, in general, generate different clusters. We also require that the number  $N$  of elements in a cluster be large enough to allow for statistical analysis, here we

have chosen  $N = 10$  elements.

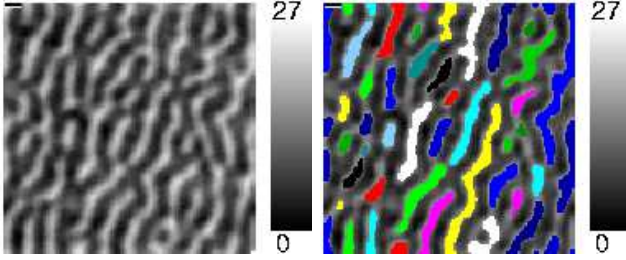


FIG. 2: (Color online) Surface profile for time 3 ions/atom (thermodynamic diffusion model,  $T = 0.2J/k_B$ ,  $L = 128$ ). The second profile contains the clusters formed from the first profile, as described in the text.

The propagation of the ripples is studied by calculating the time rate of change of the position of the centre of mass of a cluster

$$\dot{x}_{CM} = \frac{\sum_i p_i^m \dot{x}_i}{\sum_i m_i} \quad (6)$$

where the summation is over all the elements of the cluster. We have assumed a homogeneous system composed of unit mass particles, such that the center of mass of a cluster is  $x_{CM} = N^{-1} \sum_i x_i$ . The ripple wavelength is given by  $\lambda = 2\pi / k$ , being the average expectation value of the Gaussian fitted to the peak of the structure factor  $S(k) = \langle |h(k)|^2 \rangle$ , where  $h(k)$  is the Fourier transform of the height topography  $h(r;t)$ , given by

$$h(k) = \frac{1}{L^{d^0-2}} \int_r h(r;t) e^{ik \cdot r} \quad (7)$$

$d^0$  is the substrate dimension, i.e. here  $d^0 = 2$ . Fig. 2 shows two profiles of the surface for system size  $128 \times 128$  at time  $t = 3$  ions/atom; in the second profile, we print the clusters on top of their corresponding ripples. As seen in the figure of the clusters, application of periodic boundary conditions necessitates the need to first unfold toroidal clusters before calculating the position of their center of mass. As time increases, local surface slopes  $r_h$  increase, and since the non-linear effects depend on the square of  $r_h$  they will dominate by scaling down surface relaxation mechanisms [1]. These non-linear effects are responsible for the disappearance of ripples (Fig. 1) at long times, and for the transition of the surface topography from a periodic ripple pattern to a rough topography with self-affine scaling [2, 16]. We thus expect fluctuations in the position of the centre of mass due to disappearing ripples; the fluctuations are averaged out by using systems of size  $512 \times 512$  with a large number of clusters such that the ripple velocity at any time is an average of the velocities of all the ripples at this time.

#### IV. RESULTS AND DISCUSSION

The results are obtained, as already mentioned, for square lattices of size  $512 \times 512$ , with periodic boundary conditions, and as an average over fifty different realizations.

For the case of the Arrhenius diffusion mechanism, (including the Schwoebel barriers) one can choose a temperature corresponding to the physical temperature present in the experimental system. A naive guess is to use room temperature  $k_B T = 0.025$  eV, at which the experiments usually are carried through. The resulting structures are shown in Fig. 3, for intermediate as well as after long sput-

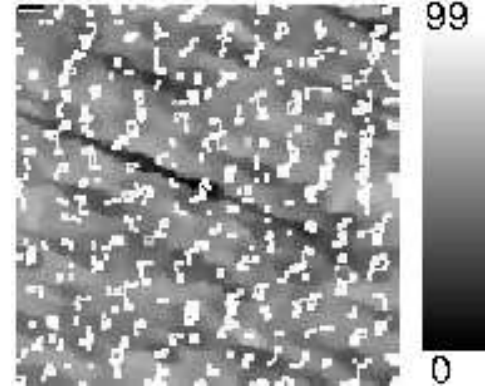


FIG. 3: Sample surface topology for a small system ( $L = 128$ ), for the Arrhenius MC diffusion mechanism at surface temperature equal to room temperature, after  $t = 100$  ions/atom. No clear ripples can be observed. Similar results were observed for almost all time, except the very early ones.

tering times. We cannot observe clean ripples. The reason is that this kind of diffusion mechanism is too slow at room temperature to effectively counteract the strong roughening due to our model of sputtering, which possesses a particularly high sputtering yield. Hops are almost always prevented if an atom has in-plane neighbors, so the mechanism is not very effective on a rough surface. Since the surface relaxation is essential for the formation of ripples [20], it needs locally higher than room temperatures to produce clean ripples in our model. This happens indeed in experiments, since most of the kinetic energy, carried by the incoming ion, is converted into lattice vibrations, hence the surface is locally strongly heated. Here, we do not know the spatio-temporal distribution of the local temperature. Either one would have to perform MD simulations, or include heat conduction in the model, both making the treatment of large systems over long time scales infeasible. Instead, we are choosing a higher but constant effective temperature  $T$ , which is a good first approximation.

Now, we want to estimate this effective temperature. The most basic approach is to describe the energy carried by the ions as a constant inflow of energy at the surface,  $\Phi$ , the temperature far away from the surface to room

temperature and solve the stationary heat-conduction equation to calculate the temperature at the surface [30]. The resulting temperature depends strongly on the ion energy, the ion current density, and the thermal conductivity of the material. For experimentally reported parameters, temperature rises up to 1500 K ( $0.155\text{eV}k_B^{-1}$ ) are found [30]. This shows that high efficient temperatures, even in the stationary state, may be achieved. However, in the experiments of Habenicht et al. [23] only small average ion current densities have been used, which result in a temperature rise at the surface of only few K.

This does not mean that one can use a temperature close to room temperature as effective temperature. The reason is that right after impact, the surface is strongly heated close to the melting temperature and the quickly cooled again, i.e. a thermal spike occurs [31]. Furthermore, the surface is sputtered using a focused ion beam (of diameter 30nm), which is moved relatively slowly over the surface and which exhibits a large spot current of  $15\text{ A/cm}^2$ . Hence, under the ion beam, for several short time intervals, surface diffusion is greatly enhanced. Marks has calculated [32] the spatio-temporal development of the temperature after ion impact by solving the dynamic heat-conduction equation, resulting in a temperature profile  $T(r;t)$  as function of time  $t$  and distance  $r$  from the point of impact. The initial distribution  $T(r;0)$  is given by a step function with  $T(r;0)$  being the melting temperature of the material for  $r < r_0$  and being the room temperature elsewhere. The initial radius  $r_0$  is determined such that the thermal energy inside this semi sphere equals to the energy carried by the ion. Marks found that the surface is heated strongly right after the impact and is cooled down to temperatures close to room temperature within few ps. Qualitatively and quantita-

parameters for ion energy and ion current density in the spot as given above, to determine an effective temperature (with  $r_0 = 15.6\text{Å}$  in our case). The basic idea is that in an time interval  $t$ , the number of hops governed by the temperature  $T(0;t)$  at the impact point should be the same as under the effective temperature  $T$ :

$$\int_0^t k_0 \exp \left( -\frac{E}{k_B T(0;t)} \right) dt = t k_0 \exp \left( -\frac{E}{k_B T} \right) : \quad (8)$$

We have neglected here the temperature dependence of  $k_0$ . When including it, we found that the resulting effective temperature changes only slightly. We have chosen  $t$ , as the average time between two ions arriving in a circle with area  $\pi r_0^2$  under the ion beam spot, resulting in  $t = 1.4 \cdot 10^{-5}\text{ps}$ . For the energy barrier, we have chosen  $E = E_{SB} + 3E_{NN} + E_S$ , which corresponds to atoms along edges of islands/steps. Using these parameters, we found an effective surface temperature of  $T = 1200\text{K}$ , i.e. considerably higher than room temperature. In this calculation it is assumed that only the energy carried by the ions hitting the "target area"  $\pi r_0^2$  contribute to the heating of the surface inside the area. If one takes into account that also the ions hitting the neighborhood of the target area contribute to the heating inside the area, even higher effective temperatures can be expected.

The exact effective temperature depends on many parameters as ion energy, ion current density, heat conduction, surface roughness etc. We are here interested only in universal effects, not in modeling a specific experimental setup. For this reason, we use the above result only as a guideline and study several temperatures of this order of magnitude and additionally above. Hence, for the further analysis of ripple movement, we consider high effective temperatures for the Arrhenius-MC model, such that the surface diffusion is indeed able to act as an effective smoothing mechanism (see Fig. 4). At such higher temperatures we observe some universal features for both diffusion mechanisms, as presented now. Figure 5 is the plot of the ripple wavelength (circle symbols) versus time measured in units of the number of ions per atom; its inset is a plot of the projection of the ripple velocity along the ion beam direction, versus time, both at the estimated effective temperature of  $k_B T = 0.1\text{eV}$  corresponding to the experimental conditions from Ref. [23].

A plot of wavelength versus time in Fig. 5 reveals that for short times  $t^{0.32}$ , which is in-between the results  $t^{0.5}$  of Habenicht et al. and  $t^{0.26}$  of Frost et al. [35]. But we observed a power-law behavior only in the initial stages of ripple formation, the wavelength becoming constant in time at the later stage.

The velocity shows a power-law behavior over a larger time interval, resulting in  $v \propto t^{0.7}$  as obtained from inset of Fig. 5. This is in excellent agreement with the experimental result  $v \propto t^{0.75}$  of Habenicht et al. [23]. A difference is that for smaller times a constant velocity was observed in the experiments, while we do not see any

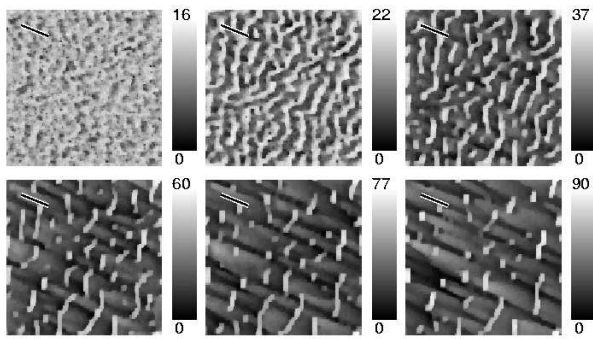


FIG. 4: Surface profiles at a substrate temperature of  $0.1\text{eV}/k_B$  with the second diffusion model. Starting from top-bottom, left-right,  $t=0.5, 1.5, 4.0, 9.0, 14.0$  and  $20.0$  ions/atom. In both cases, depicted here and in Fig. 1, ripples propagate along a direction opposite to that of the ion beam.

tively similar profiles have been observed in MD simulations [33] as well. We apply this equation, using the

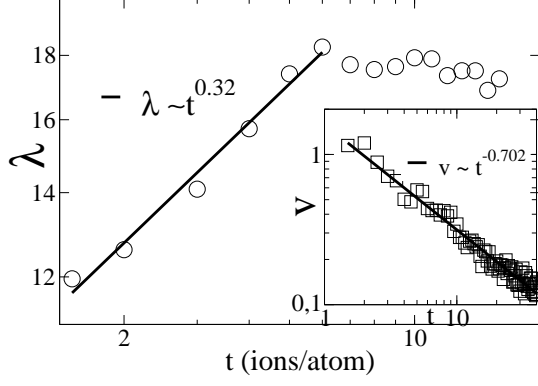


FIG. 5: Ripple wavelength,  $\lambda$ , measured in lattice units, as a function of time,  $t$ . The inset shows the time dependence of the ripple propagation velocity,  $v$  (measured in lattice units per ion per atom). Both results are for the kinetic diffusion mechanism, at a substrate temperature of  $k_B T = 0.1 \text{ eV}$ .

clean ripples for smallertimes than the power-law regime. Anyway, combining both scaling results gives  $v \sim t^{-2.19}$ , in good agreement with the exponent  $-2$  of continuum theory [2].

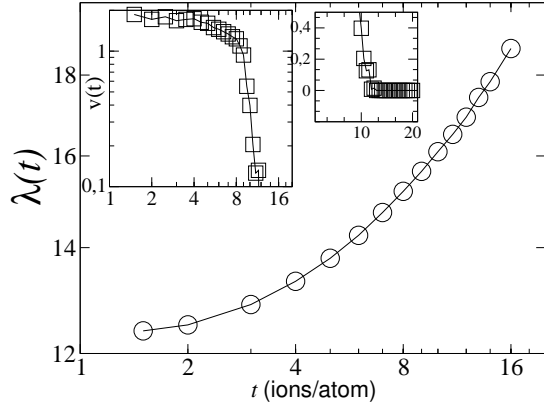


FIG. 6: Ripple wavelength,  $\lambda$ , measured in lattice units, as a function of time,  $t$ . The inset shows the time dependence of the ripple propagation velocity,  $v$  (measured in lattice units per ion per atom). Both results are for the thermodynamic diffusion mechanism, at a substrate temperature of  $0.2 \text{ J k}_B^{-1}$ .

Now we turn to higher effective substrate temperatures, corresponding e.g. to higher ion currents and/or materials with lower heat-conductivity. Figures 6 and 7 are plots of the ripple wavelength (circle symbols) as a function of time, at respective temperatures  $k_B T = 0.2 \text{ J}$  and  $k_B T = 0.2 \text{ eV}$ ; using the first and second models of surface diffusion respectively. In both models, the ripples

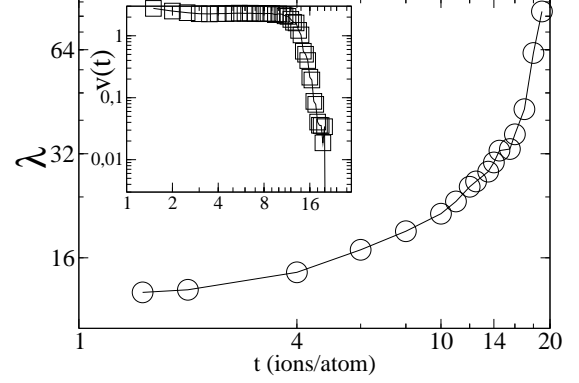


FIG. 7: Same plot as in Fig. 6 but for the Arrhenius diffusion mechanism, for a substrate temperature of  $0.2 \text{ eV} = k_B$ . In both figures, the line with circle symbols represent the wavelength while the line with square symbols represent the velocity.

disappear after a while, i.e. the ripple wavelength diverges. Considering the lifetime of the ripples from first appearance to annihilation, the wavelength increases exponentially with time as  $\exp(t)$ ,  $\lambda = 0.029$  (Fig. 6), in the first model, while it increases with time according to the inverse law  $\lambda(t)^{-1} = (c_1 - c_2 t)$  with  $c_1 = 0.083$  and  $c_2 = 0.0036$  (Fig. 7) in the second model. To investigate the origin of the difference, we performed also simulations with the Arrhenius model, but with the Schwoebel term set to zero. In this case the result was very similar to result in Fig. 6 of the thermodynamic model (which has no Schwoebel term here), and we obtained a behavior  $\exp(0.036t)$ . On the other hand, when we set the energy in the Schwoebel term to twice its value,  $E_{SB} = 0.3 \text{ eV}$ , the result is very similar to  $E_{SB} = 0.15 \text{ eV}$ . This shows that the Schwoebel barrier plays an important role in the pattern formation process. Note that these results are purely heuristic. We are not aware of any theory of the time dependence of ripple wavelength and velocity, only a calculation of the dispersion relation  $v(k)$  has been performed within linear theory [2]. Furthermore, there exists an analytic study of the temporal development of step bunches during epitaxial growth [22, 34].

The insets of Figs. 6 and 7 are plots of the ripple velocity (line with square symbols) as a function of time. Irrespective of which surface diffusion mechanism is employed, the velocity is at first almost independent of time, then it disperses after a transition time  $t_r$ . This initial plateau is similar to the plateau observed in the experiments, but the drop in velocity is very abrupt, no clear power law is visible then. Moreover, the ripples finally come to rest before completely disappearing, as seen in the smaller inset of Fig. 6. We find, however, that at the lower temperature in the kinetic model, the ripples do not stop moving until their disappearance. Figure 8 shows the dependence of the ripple velocity on the wave-

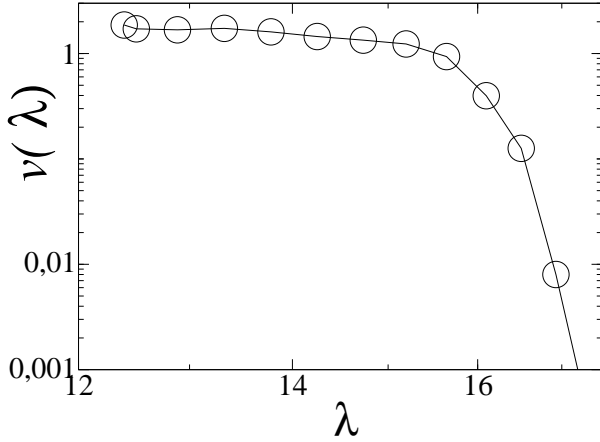


FIG. 8: Ripple velocity as a function of ripple wavelength, for the thermodynamic and, in the inset, for the Arrhenius surface diffusion mechanism.

length for  $k_B T = 0.2 \text{ eV}$  resp  $0.2 \text{ J}$ , their order of magnitude relationship is about the same as in the experiment. We see in Fig. 9 that the trend in velocity variation is the same at high temperatures but the magnitude increases with temperature, as one would expect from the temperature dependence of the surface diffusion. But we only observed a power-law scaling at temperatures below  $k_B T = 0.18 \text{ eV}$ . This indicates that the presence of power-law scaling of ripple wavelength and velocity, and the corresponding exponents, depend on the time scale of observation (Fig. 5), as well as on the effective temperature.

It seems that the increase in magnitude of the velocity, when measured at same time ( $t < t_c$ ) but different temperatures, does not continue indefinitely in our model. In the upper graph of Fig. 9 there is very little difference in the magnitudes of the velocity at temperatures  $2.0$  and  $5.0 \text{ J k}_B^{-1}$ ; even though the temperature difference is very high. This saturation behaviour is also displayed in the ripple wavelength at the same higher temperatures, as seen in the lower graph of Fig. 9. In principle, one can still fit an exponential law to the data, except that the decay constant in the exponential becomes very small (It has the respective values of  $0.029$ ,  $0.018$ ,  $0.0031$ , and  $0.003$  from the lowest to the highest temperature.). So for very high effective temperatures we could equally well fit a power-law. Hence, there may be some "critical substrate temperature", above which the wavelength remains nearly constant in time; and the velocity, after some time  $t_c$ , drops instantaneously to zero. Nevertheless, the temperature where such a "transition" will take place, is probably unphysically high (see below), so that the material used in the experiment would start to evaporate before reaching this point. But other materi-

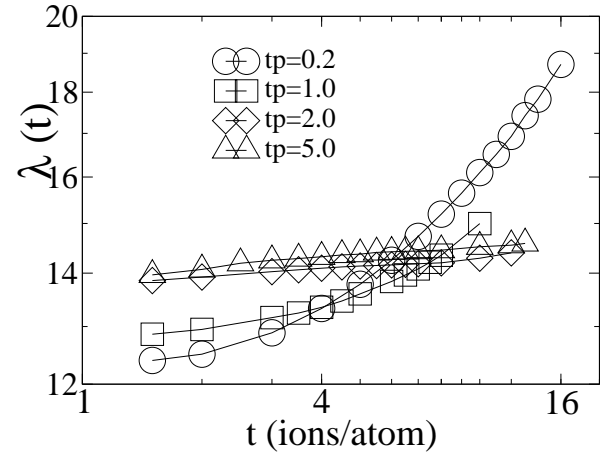
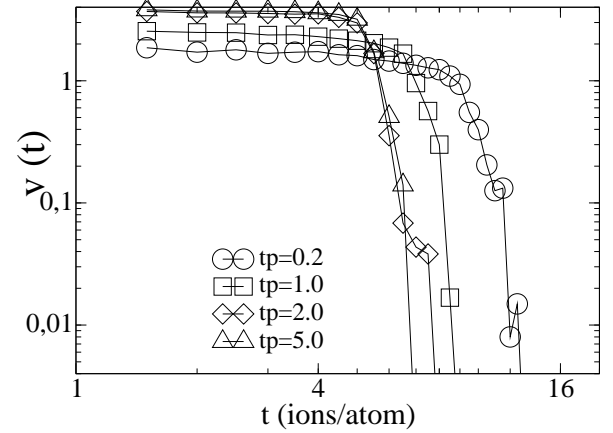


FIG. 9: Temperature dependence of the ripple velocity (upper graph), and ripple wavelength (lower graph); for the thermodynamic diffusion mechanism. Temperature is in units of  $\text{J k}_B^{-1}$ .

als, in combination with high ion currents, might quite display such a behavior. So far, we are only aware of one set of experiments [23]. Hence, it would be very interesting to see, whether some temperature dependence of the dynamical features, including the disappearance of the coarsening, can be seen in experiments at higher effective temperatures corresponding to high ion currents and/or higher lab temperatures.

Our results for the second diffusion model also indicate that in  $\langle t \rangle = (c_1 - c_2 t)$ ,  $c_2$  approaches zero with increasing temperature. Here, where we can measure the temperature in real units, it is clear that the "transition" to almost non-coarsening ripples, takes place at unrealistically high temperatures  $2 - 5 \text{ eV} / k_B$ , where the material starts to evaporate. Moreover, we notice in Fig. 9 that the transition time from linear regime to onset of non-

linearities decreases with increasing temperature.

To summarize, ripple propagation depends on the effective substrate temperature as well as the diffusion mechanism. At around so-far experimentally realized temperatures, ripples propagate, from first appearance, with decreasing velocity until disappearance without full cessation of motion. At high effective temperatures, however, immediately after ripple formation, the ripples move with constant velocity for some time, after which they begin to decelerate (insets of Figs. 6, 7) and after some time, depending on the diffusion model, the ripples stop moving but keep disappearing gradually. At the same time the ripple structure is gradually being washed out, and in the final stage the ripples are completely wiped out. The ripple wavelength is always increasing in time at high temperatures, while at low effective temperatures it initially increases with time, and later becomes constant.

## V. CONCLUSION AND OUTLOOK

We have studied the propagation of ripples by means of a discrete  $(2+1)$ -dimensional model of the sputtering process, combined with one of two different solid-on-solid models of surface diffusion: a Arrhenius-MC mechanism with Ehrlich-Schwobell barriers and a thermodynamic mechanism without a Schwobell term. We have obtained the formation and propagation of the ripples with both diffusion mechanisms used in turn. Furthermore, we have obtained the same trend in the behavior of ripple velocity and wavelength as observed experimentally and predicted theoretically, but, in addition to the experimental results, we find a drastic change in the ripple propagation at temperatures well above the so-far experimentally realized effective temperature; for instance we found deviations from power-law into exponential or inverse-law behavior, and in addition, the ripples first stop moving before vanishing completely. We find that, at very high effective temperatures, the behavior of the ripple velocity is characterized by two regions, separated at the transition time. In the first region it is constant and in the second region it decreases rapidly to zero. Between the two regions a power-law dependence can be observed for some small time interval. Whereas, around so-far experimentally realized temperature, the velocity-time relationship obeys a power-law. Furthermore, at high effective temperatures, the wavelength increases exponentially with time in the thermodynamic diffusion model (and in the Arrhenius diffusion model without Schwobell term) and obeys an inverse law for the Arrhenius model including the Schwobell barrier. In addition, we find further strong dependencies on the effective substrate temperature; as the temperature increases the magnitude of the veloc-

ity also increases. The transition time between constant and decreasing velocity is also found to decrease with increasing temperature. Our results indicate an approach towards a saturation behaviour of velocity or wavelength with increasing effective substrate temperature, where the wavelength is expected to become time independent. However, this may happen at an unphysically high temperature. Anyway, an experimental study of the dependence of the dynamical features of ripple formation and agreement on the physical conditions seems very promising.

One open problem of our model, at high incidence angles (e.g.  $\theta > 75^\circ$ ), is that it uses the Sigmund formula for modeling the sputtering process. In a recent simulation [36] using a binary collision approximation, we observed that close to the penetration point of the ion, much less atoms were sputtered than predicted by the Sigmund formula (1), in fact the distribution shows a minimum there. When incorporating this effect in the Bradley-Harper linear theory [20] of sputtering, one e.g. observes [36] that the sputter yield, i.e. the number of removed atoms per ion, exhibits a minimum for grazing incidence, like in experiments, in contrast to the original linear theory [20]. Hence, it may be promising to apply a different formula describing the sputtering, which takes into account this effect.

Furthermore, the role of the interplay between the surface diffusion process and the sputtering process is still not fully understood. So far, we know that including a pure  $T = 0$  relaxation in our sputtering model does not [24] lead to a disappearance of ripples for long times. Next, we know from this study, that one approach including calibrated Schwobell barriers does not yield ripples at room temperature for sputtering yield  $Y \approx 7$ . There are several different models [27, 28, 37, 38, 39, 40, 41, 42] for surface diffusion, which could be combined in a construction kit manner. Here, an extensive study over different combinations of parameters is necessary.

Finally, it would be of interest to include crystal anisotropy into the surface diffusion; This may give results in agreement with experimental studies of metallic substrates, which may be useful in understanding the anomalies of such surfaces.

Acknowledgements: The authors would like to thank K. Lieb and R. Cuerno for helpful discussions and suggestions. OEY thanks Henning Lowe for interesting discussions. The large scale numerical simulations were performed on the workstation clusters of the institute. This work was funded by the DFG (Deutsche Forschungsgemeinschaft) within the SFB (Sonderforschungsbereich) 602 and by the VolkswagenStiftung (Germany) within the program "Nachwuchsgruppen an Universitäten".

---

[1] A. -L. Barabasi and H. E. Stanley, *Fractal Concepts in Surface Growth* (Cambridge University Press, Cambridge,

1995).



- [2] M. M. Makeev, R. Cuerno and A. -L. Barabasi, Nuc. Instr. and Meth. in Phys. Res. B 197, 185 (2002).
- [3] S. Facsko, T. Dekorsy, C. Koerdt, C. Trappe, H. Kurz, A. Vogt, and H. L. Hartnagel, Science 285, 1551 (1999).
- [4] T. M. Mayer, E. Chason, and A. J. Howard, J. Appl. Phys. 76, 1633 (1994).
- [5] E. Chason, T. M. Mayer, B. K. Kellemann, D. T. McClroy, and A. J. Howard, Phys. Rev. Lett. 72, 3040 (1994).
- [6] C. M. Demanet, J. B. Malherbe, N. G. Vandenberg, and V. Sankar, Surf. Interface Anal. 23, 433 (1995).
- [7] S. W. McLaren, J. E. Baker, N. L. Finnegan, and C. M. Loxton, J. Vac. Sci. Technol. A 10, 468, (1992).
- [8] J. B. Malherbe, CRC Crit. Rev. Solid State Mater. Sci. 19, 55 (1994), and references therein.
- [9] G. Carter, and V. V. Ishnyakov, Phys. Rev. B 54, 17647 (1996).
- [10] J. Erlebacher, M. J. Aziz, E. Chason, M. B. Sinclair, and J. A. Florio, Phys. Rev. Lett. 82, 2330 (1999) and references therein.
- [11] S. Habenicht, W. Bolse, K. P. Lieb, K. Reimann, and U. Geyer, Phys. Rev. B 60, R2200 (1999).
- [12] According to the linear theory of Bradley and Harper,  $\phi_1(\theta) = -fs \frac{c}{2} [1 + \frac{sc(\frac{c}{2})}{2} \beta + \gamma]$  and  $\phi_2(\theta) = \frac{c}{2} f_1 + \frac{s(\frac{c}{2})}{2} g$ ; where  $s = \sin^2(\theta)$ ,  $c = \cos^2(\theta)$ ,  $\beta = (\frac{d}{\lambda})^2$ ,  $\gamma = (\frac{d}{\lambda})^2$ ,  $f = s + c$ ,  $g = \frac{2s}{d}$ , and are as described in this paper. Depending on the choice of  $\theta$  and  $\lambda$  there may be two critical angles [20].
- [13] S. Rusponi, C. Boragno, and U. Valbusa, Phys. Rev. Lett. 78, 2795 (1997).
- [14] S. Rusponi, G. Costantini, C. Boragno, and U. Valbusa, Phys. Rev. Lett. 81, 2735 (1998).
- [15] S. Rusponi, G. Costantini, C. Boragno, and U. Valbusa, Phys. Rev. Lett. 81, 4184 (1998).
- [16] E. A. Eklund, R. Bruinsma, J. Rudnick, and R. S. Williams, Phys. Rev. Lett. 67, 1759 (1991).
- [17] E. A. Eklund, E. J. Snyder, and R. S. Williams, Surf. Sci. 285, 157 (1993).
- [18] J. Krim, I. Heyvaert, C. Van Haesendonck, and Y. Bruynseraede, Phys. Rev. Lett. 70, 57 (1993).
- [19] H. -N. Yang, G. -C. Wang, and T. -M. Lu, Phys. Rev. B 50, 7635 (1994).
- [20] R. M. Bradley and J. M. E. Harper, J. Vac. Sci. Technol. A 6, 2390, (1988).
- [21] R. Cuerno and A. -L. Barabasi, Phys. Rev. Lett. 74, 4746 (1995).
- [22] A. Pimpinelli, V. Tonchev, A. Videcoq, and M. Vladimirova, Phys. Rev. Lett. 88, 206103 (2002).
- [23] S. Habenicht, K. P. Lieb, J. Koch, and A. D. Wieck, Phys. Rev. B 65, 115327 (2002).
- [24] A. K. Hartmann, R. Kree, U. Geyer, and M. Kolbel, Phys. Rev. B 65, 193403 (2002).
- [25] P. Sigmund, Phys. Rev. 184, 383 (1969).
- [26] J. F. Ziegler, J. P. Biersack and K. Littmark, The Stopping and Range of Ions in Matter, (Pergamon, New York 1985); see also <http://www.srim.org/>.
- [27] M. Siegert and M. P. Lischke, Phys. Rev. E 50, 917 (1994).
- [28] P. Smilauer, M. R. Wilby, and D. D. Vvedensky, Phys. Rev. B 47, 4119 (1993).
- [29] T. Shitara, D. D. Vvedensky, M. R. Wilby, J. Zhang, J. H. Neave, and B. A. Joyce, Phys. Rev. B 46, 6815 (1992).
- [30] J. Mengalis, J. Vac. Sci. Technol. B 5, 469 (1987).
- [31] W. Primak, Phys. Rev. 98, 1854 (1955).
- [32] N. A. Marks, Phys. Rev. B 56, 2441 (1997).
- [33] D. Saada, J. Adler, and R. K. Alish, Phys. Rev. B 59, 6650 (1999).
- [34] The growth equation studied in Ref. 22 is very different from the equations describing sputtering, self-similar behavior instead of periodic structures were studied, and the average terrace width decreases with time, while the wavelength increases in our case.
- [35] F. Frost, A. Schindler, and F. Bigl, Phys. Rev. Lett. 85, 4116 (2000).
- [36] M. Feix, A. Hartmann, R. Kree, J. Muñoz-García, and R. Cuerno, to appear in Phys. Rev. B, preprint cond-mat/0407245.
- [37] S. DasSarma and P. Tamborenea, Phys. Rev. Lett. 66, 325 (1991).
- [38] M. R. Wilby, D. D. Vvedensky, and A. Zangwill, Phys. Rev. B 46, 12896 (1992); 47, 16068 (E) (1993).
- [39] M. V. Ramana Murthy and B. H. Cooper, Phys. Rev. Lett. 83, 352 (1999).
- [40] K. Malarz and A. Z. Maksymowicz, Int. J. Mod. Phys. C 10, 659 (1999).
- [41] S. V. Ghaisas, Phys. Rev. E 63, 062601 (2001).
- [42] P. Punyindu Chatrathom, Z. Toroczka, and S. DasSarma, Phys. Rev. B 64, 205407 (2001).